Ohmic-Viscous Dissipation in MHD Slip Flow of Cu-blood Nanofluid over a Stretching Surface along Nanoparticle Shapes

Santosh Chaudhary* & Kiran Kunwar Chouhan

Department of Mathematics, Malaviya National Institute of Technology, Jaipur-302 017, India

MHD nanofluid has been of great importance due to its influential thermal aspects. Present study involves two dimensional MHD boundary layer slip flow of Cu-blood nanofluid towards a linearly stretching sheet under impact of Ohmic heating, viscous dissipation and suction/injection process. Influence of various shapes of Cu nanoparticles on temperature has also been taken into consideration. Governing partial differential equations have been converted into non-dimensional form through suitable similarity transformations and solved numerically via special spectral relaxation method (SRM). Effect of emerging parameters, suction/injection parameter, velocity slip parameter, solid volume fraction, magnetic parameter, Brinkman number and shape factor have been explored and described graphically. Numerical values of shear stress and heat flux have been reported via table and influence of controlling parameters have also been analysed on skin friction coefficient and Nusselt number. Subsequently, the validation of the results has been established through comparison with previously published data. The results of this investigation can be applicable in biomedical fields.

Keywords: Ohmic heating, Viscous dissipation, MHD, Slip condition, Nanofluid, Stretching surface

1 Introduction

The irreversible processes– viscous dissipation and Ohmic heating demonstrate the transformation of kinetic and electrical energy into thermal energy, respectively. Energy viscous dissipation is the work done by the fluid on adjacent layers along with the shear forces action, while Ohmic heating, also known as Joule heating, is a mechanism in which conduction electrons, due to collision procedure, transfer into the atoms of conductor. Usually, viscous dissipation effect is considered during the high flow velocity or high viscosity of the fluid. Viscous dissipation is of interest for its applications such as cooling of reactors in nuclear engineering, natural convection in several devices, extrusion processes in food and polymer industries and also in powerful gravitational field processes. Joule heating also has a variety of usage in electric heating devices, fuse wire, electronic cigarette, electric bulb, system of power generator, metallic sheet cooling processes, *etc.* Abo-Eldahab and El Aziz[1] presented the influence of viscous dissipation and Joule heating on a magneto hydro dynamic flow over a flat plate due to Hall and ion-slip currents. Palani and Kim[2] discussed the combined effect of Joule heating and viscous dissipation on an MHD-free convection flow over a semi-infinite plate with varying surface temperature. Hayat *et al.*[3] discussed the impact of viscous dissipation and Joule heating on a non-uniform melting heat transfer in MHD boundary layer flow of Cu-water nanofluid. Chaudhary and Choudhary[4] stated viscous dissipation and Joule heating effect on a two-dimensional MHD flow and heat transfer due to a flat surface in motion. Aly and Pop[5] studied the heat transfer and MHD flow near a stagnation point past a stretching/shrinking sheet in presence of viscous dissipation. Recently, Zhang *et al.*[6] depicted an MHD stagnation-point flow of Fe_3O_4/water nanofluid towards a curved stretching/shrinking sheet with Joule heating and convective boundary condition.

MHD (magnetohydrodynamics) concerns the tendency of electrically conducting fluids towards the forces exerted by magnetic field. Such conducting fluids involve solar collectors, blood plasmas, liquid metals, *etc.* It plays an essential role in interpreting natural phenomena like star formation, interaction of solar wind with Earth's magnetic field, determination of corona structure. A widespread application of MHD flow can be seen in chemical engineering, electromagnetic casting, magnetohydro-dynamic sensors, stellar, geo-physics, metallurgical industries and medical science. Exertion of magnetic

---

*Corresponding author: (E-mail: d11.santosh@yahoo.com)

field in MHD is being used in many processes such as fusion of metals in an electrical furnace, extenuation of blood flow or reduction of tissue temperature during surgery, MRI scanner for cancer tumour treatment. The Nobel Laureate Alfvén[7] investigated the existence of MHD waves and analysed the MHD field. There has been extensive research on MHD flow owing to its broad scope of applications. For instance, Abo-Eldahab and Salem[8] analysed a free-convection magnetohydrodynamic flow of non-Newtonian power-law fluid over a stretching surface. A modified differential transform method to solve the MHD boundary layer equations was proposed by Rashidi[9]. In addition, Kechil and Hashim[10], Jat and Chaudhary[11], Misra and Sinha[12], Chaudhary and Kumar[13], Mabood et al.[14] and Khan et al.[15] have depicted their studies in various aspects regarding MHD flow. Abdel-Wahed and Emam[16] covered hall current effect on MHD flow of nanofluid in presence of Joule heating and viscous dissipation over a rotating disk. Recently, *Waini et al.*[17] observed heat transfer and MHD flow of a hybrid nano-fluid along with the radiation effects over a permeable stretching/shrinking wedge.

The phenomenon of non-adhesion of the fluid to the wall is referred as velocity slip. The no-slip boundary condition is no longer valid as it is a hypothesis instead of a condition inferred from any principle, therefore its validity has been persistently questioned in the scientific literature. Due to significance of the slip effect on the boundary layer flows of fluids, a principled analysis has been done in this study. Martin and Boyd[18] investigated slip effect on momentum and heat transfer in boundary layer flow over a plate. Zhu et al.[19] addressed slip condition impact on MHD stagnation point flow over a stretching surface. Recently, Seth and Mishra[20], Chaudhary and Choudhary[21], Tabassum and Mustafa[22] and Murthy[23] carried out analysis on velocity slip effect.

Thermal conductivity of fluids has a major influence on heat transfer performance. Usual base fluids have inadequate efficacy in heat transfer, so in order to reduce this limitation a novel method as nanofluid has been used during last decade. Nanofluid is a colloidal suspension created by dispersion of ultra-fine particles in traditional base fluid. These ultra-fine particles are objects with diameter between 1 to 100 nanometres, usually consist of metals, oxides, nitrides, carbides or carbon nanotubes. Nanofluids due to their remarkable merits such as higher conductivity, less pumping capacity, low flow

path interruption and high stability have a high competence to be used to improve heat transfer mechanism. Choi and Eastman[24] firstly proposed the term nanofluid. Later, Xuan and Li[25] investigated flow features and convective heat transfer of nanofluids. Further several researchers like Khanafer et al.[26], Gümgüm and Tezer-Sezgin[27], Khan and Pop[28], Mahmoodi and Hashemi[29] and Sheikholeslami et al.[30] proposed various problems on nanofluids and nanoparticles in different aspects. Turkyilmazoglu[31] stated correspondence between nanofluid flows and standard fluid flows. Su[32] investigated the Hall and ion-slip effects on time dependent MHD flow of Cu-water nanofluid through a vertical stretching plate. Daniel et al.[33] considered MHD flow of the nanofluid with thermal radiation effect due to a nonlinear stretching surface of variable thickness. Chaudhary and Kanika[34] investigated heat transfer and Marangoni driven MHD flow of CNT-water nanofluid in presence of viscous dissipation, Joule heating and radiation effects.

The fluid flow over a stretching sheet is of considerable interest due to its ever-rising industrial applications and important usage in many technological processes. Some of them are polymer extrusion from a dye, oil recovery and drawing strips in cooling process. Cortell[35] examined an electrically conducting power-law fluid flow past a stretching sheet in presence of uniform magnetic field. Ibrahim and Shankar[36] discussed the impact of velocity slip and thermal radiation on magnetohydrodynamic flow and heat transfer due to a nanofluid over a stretching permeable sheet. Moreover, Khader and Megahed[37], Khan et al.[38], Nadeem and Khan[39], Chaudhary and Kanika[40] and Jabeen et al.[41] also explored MHD flow over stretching surface.

The current study is inspired by the work done by Jafari and Freidoonimehr[42], under the impact of viscous dissipation and Ohmic heating which were neglected in their studies. Moreover, this work is also extended for different shapes of copper (Cu) nano-particles with base fluid human blood. The spectral relaxation method (SRM) is employed to solve the ordinary differential equations. The novelty of the present study can be perused in terms of viscous dissipation and Ohmic heating effects. To the best of authors' knowledge, there is no investigation in literature, communicating these effects on Cu-blood nanofluid by considering suction/injection and slip condition for five diverse shapes of nanoparticles. The applications of this investigation can involve further

modifications in respect of biology, medicine and biotechnology, for instance, blood flow in micro-circulatory system and more specifically drug delivery (Dinarvand et al.[43], Tripathi et al.[44]).

2 Mathematical modeling

A two-dimensional magnetohydrodynamic boundary layer flow over a stretching surface in a Cu-blood nanofluid due to its various particle shapes is considered. The coordinate system (x, y) is introduced such that the $x-$ axis expresses the direction of motion of the stretching sheet while $y-$ axis is orthogonal to the sheet. The geometrical coordinates and the physical model of the problem is shown in Fig. 1. In addition, the following conditions are also taken into account

(i) The flow is steady, laminar and incompressible.
(ii) Nanoparticles are assumed to have thermal equilibrium with base fluid- blood.
(iii) u and v are the velocity constituents in x and y directions, respectively.
(iv) The surface temperature $T_w = T_\infty + bx$ is a linear function of x, where T_∞ denotes the ambient temperature of the nanofluid and b is the positive constant.
(v) It is assumed that the stretching velocity of the sheet is $u_w = ax$ where a is stretching rate constant. Magnetic field of constant strength B_0 is applied to the sheet besides induced magnetic field is neglected due to very small magnetic Reynolds number.

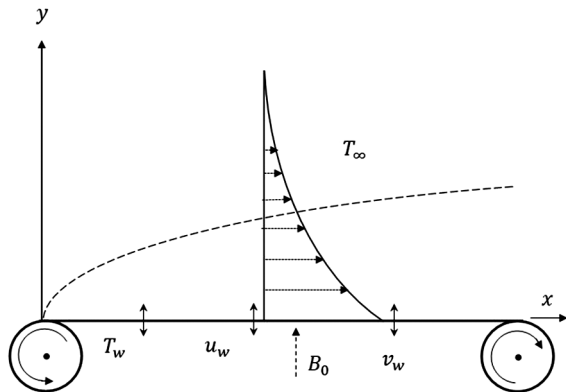The governing equations, under the above-described assumptions, are as follows (Jafari and Freidoonimehr[42])

Fig. 1 — Physical model and geometric coordinates.

$$\frac{\partial u}{\partial x} + \frac{\partial v}{\partial y} = 0 \qquad \text{... (1)}$$

$$u\frac{\partial u}{\partial x} + v\frac{\partial u}{\partial y} = \frac{1}{\rho_{nf}}\left[\mu_{nf}\frac{\partial^2 u}{\partial y^2} - (\sigma_e)_{nf} B_0^2 u\right] \qquad \text{... (2)}$$

$$u\frac{\partial T}{\partial x} + v\frac{\partial T}{\partial y} = \frac{1}{(\rho C_p)_{nf}}\left[\kappa_{nf}\frac{\partial^2 T}{\partial y^2} + \mu_{nf}\left(\frac{\partial u}{\partial y}\right)^2 + (\sigma_e)_{nf} B_0^2 u^2\right] \qquad \text{... (3)}$$

The appropriate boundary conditions for aforementioned equations are

$$y = 0 : u = u_w + u_{slip}, v = v_w, T = T_w$$
$$y \to \infty : u \to 0, T \to T_\infty \qquad \text{... (4)}$$

In the above equations, subscript nf indicates the nanofluid, $\rho = \frac{\mu}{v}$ is the density, μ is the coefficient of viscosity, v is the kinematic viscosity, σ is the electrical conductivity, T is the temperature of the nanofluid, C_p is the specific heat at constant pressure, κ is the thermal conductivity, $u_{slip} = A\frac{\partial u}{\partial y}$ is the slip velocity, A is the slip velocity constant and v_w is the mass transfer velocity perpendicular to the stretching sheet with suction when $v_w > 0$ or injection when $v_w < 0$. In the present study, only suction effect is considered through the sheet. Thermo-physical properties of the nanofluid and nanoparticles are given in Table 1.

The expressions for the nano-fluid parameters density, viscosity, electrical conductivity, heat capacity and thermal conductivity are given by Mohammad and Kandasamy[45]

$$\rho_{nf} = (1-\phi)\rho_f + \phi\rho_s \qquad \text{... (5)}$$

$$\mu_{nf} = \frac{\mu_f}{(1-\phi)^{5/2}} \qquad \text{... (6)}$$

$$(\sigma_e)_{nf} = \frac{2(\sigma_e)_f + (\sigma_e)_s - 2\phi[(\sigma_e)_f - (\sigma_e)_s]}{2(\sigma_e)_f + (\sigma_e)_s + \phi[(\sigma_e)_f - (\sigma_e)_s]}(\sigma_e)_f \qquad \text{... (7)}$$

$$(\rho C_p)_{nf} = (1-\phi)(\rho C_p)_f + \phi(\rho C_p)_s \qquad \text{... (8)}$$

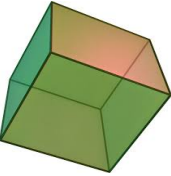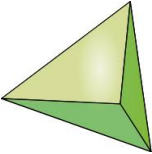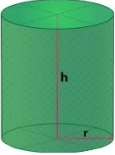Table 1 — Thermo-physical properties of base fluid and nanoparticles.

Physical properties	$\rho(kg/m^3)$	$\sigma_e(S/m)$	$C_p(J/kg\,K)$	$\kappa(W/mK)$
Human blood	1053	0.800	3594	0.492
Cu	8933	5.96×10^7	385	400

$$\kappa_{nf} = \frac{\left[(m-1)\kappa_f + \kappa_s\right] - (m-1)\phi(\kappa_f - \kappa_s)}{\left[(m-1)\kappa_f + \kappa_s\right] + \phi(\kappa_f - \kappa_s)}\kappa_f \qquad \dots (9)$$

where, subscripts f and s represent base fluid and solid nano-particles, respectively, ϕ is the solid volume fraction parameter, $m = \dfrac{3}{\zeta}$ refers to the empirical shape factor and ζ is the sphericity of the particles. Sphericity is proportion of the surface area of a sphere to the surface area of a particle having same volume as that of sphere. The value of sphericity ζ for sphere is unity and less than unity for an irregular shaped particle. Table 2 shows different shapes of Cu nanoparticles namely sphere, tetrahedron, hexahedron, cylinder and lamina, and corresponding values of sphericities which are considered in the study.

Table 2 — Nanoparticle shapes with corresponding values of sphericity.

Model	Shape	ζ
Sphere		1.0000
Hexahedron		0.8060
Tetrahedron		0.7387
Cylinder		0.4710
Lamina		0.1857

3 Similarity analysis

Dimensionless similarity transformation variables for the current problem by Jafari and Freidoonimehr[42] are as follows

$$\psi = \sqrt{av_f}\,xf(\eta), \qquad \eta = \sqrt{\frac{a}{v_f}}\,y, \qquad T = T_\infty + (T_w - T_\infty)\theta(\eta) \qquad \dots (10)$$

where, $\psi(x, y)$ is the stream function that clearly satisfies the mass conservation Eq. (1) with $u = \dfrac{\partial\psi}{\partial y}$ and $v = -\dfrac{\partial\psi}{\partial x}$. $f(\eta)$ is the non-dimensional stream function, η is the similarity variable and $\theta(\eta)$ is the non-dimensional temperature.

Using the similarity variables Eq. (10) in Eqs (2)–(4), the governing boundary layer equations are transformed as

$$f''' + (1-\phi)^{5/2}\left(1-\phi+\phi\frac{\rho_s}{\rho_f}\right)\left(ff'' - f'^2\right)$$
$$-\frac{(\sigma_e)_{nf}}{(\sigma_e)_f}(1-\phi)^{5/2}Mf' = 0 \qquad \dots (11)$$

$$\frac{\kappa_{nf}}{\kappa_f}\theta'' + \Pr\left[1-\phi+\phi\frac{(\rho C_p)_s}{(\rho C_p)_f}\right]\left(f\theta' - f'\theta\right)$$
$$+ Br\frac{1}{(1-\phi)^{5/2}}\left[f''^2 + \frac{(\sigma_e)_{nf}}{(\sigma_e)_f}(1-\phi)^{5/2}Mf'^2\right] = 0 \qquad \dots (12)$$

with the associated boundary

$$\eta = 0: f = f_w,\ f' = 1 + \lambda f'',\ \theta = 1$$
$$\eta \to \infty: f' \to 0,\ \theta \to 0 \qquad \dots (13)$$

where, primes refer to the derivatives of functions with respect to η, $M = \dfrac{(\sigma_e)_f B_0^2}{a\rho_f}$ is the magnetic parameter, $\Pr = \dfrac{(\rho C_p)v_f}{\kappa_f}$ is the Prandtl number, $Br = \Pr Ec$ is the Brinkman number, $Ec = \dfrac{u_w^2}{(C_p)_f(T_w - T_\infty)}$ is the Eckert number, $f_w = -\dfrac{v_w}{\sqrt{av_f}}$ is the suction/injection parameter and $\lambda = A\sqrt{\dfrac{a}{v_f}}$ is velocity slip parameter.

4 Declaration of curiosity

Physical parameters of interest are local skin friction coefficient C_f and local Nusselt number Nu_x, expressed as:

$$C_f = \frac{\mu_{nf}\left(\frac{\partial u}{\partial y}\right)_{y=0}}{\frac{\rho_f u_w^2}{2}} \qquad \text{... (14)}$$

$$Nu_x = -\frac{\kappa_{nf} x\left(\frac{\partial T}{\partial y}\right)_{y=0}}{\kappa_f (T_w - T_\infty)} \qquad \text{... (15)}$$

Above, both of the parameters are in dimensionless form. By employing the non dimensional transformation Eq. (10), Eqs (14) and (15) can be converted as follows

$$\sqrt{Re_x}\,C_f = \frac{2}{(1-\phi)^{5/2}} f''(0), \quad \frac{1}{\sqrt{Re_x}} Nu_x = -\frac{\kappa_{nf}}{\kappa_f}\theta'(0) \quad \text{... (16)}$$

where, $Re_x = \dfrac{u_w x}{\nu_f}$ is the local Reynolds number.

5 Numerical method

In this section, an algorithm called Spectral Relaxation Method (SRM) is employed to solve the system of non-linear ordinary differential Eqs (11) and (12) with boundary conditions Eq. (13). SRM is a useful technique to deal with similarity variable boundary layer flow problems having exponentially decaying profiles. The strategy of Gauss-Seidel method of decoupling the system of equation is employed to derive the iteration scheme. Further, the Chebyshev-Pseudo Spectral method is utilized to solve this decoupled system of equations.

Approximation of the derivatives of unknown similarity variables at the collocation points is done through differentiation matrix D as matrix vector product[46]

$$\frac{df}{d\eta} = \sum_{k=0}^{N} D_{lk} f(\tau_k) = Df, \qquad l=0,1,2,...,N \qquad \text{... (17)}$$

where, $N+1$ is the number of mesh points (collocation points), $D = \dfrac{2D}{\eta_\infty}$ is differentiation matrix of order $(N+1)\times(N+1)$ and $f = [f(\tau_0), f(\tau_1),...,f(\tau_N)]^T$ is the vector function at the mesh-points. η_∞ is a confined length chosen with an initial guess and increment is done with the further steps to approximate the circumstances of the governing problem at infinity and variable τ is used in order to transform the interval $[0,\eta_\infty]$ to the interval $[-1,1]$ on

which SRM is executed. Higher order derivatives can be obtained with powers of D

$$f^n = D^n f \qquad \text{... (18)}$$

where, n refers to the order of derivative. The transformation $f' = g$ is applied to reduce the order of momentum Eq. (11), in order to implement spectral method on Eqs (11)–(13).

$$g'' + (1-\phi)^{5/2}\left(1-\phi+\phi\frac{\rho_s}{\rho_f}\right)(fg'-g^2) - \frac{(\sigma_e)_{nf}}{(\sigma_e)_f}(1-\phi)^{5/2}Mg = 0 \quad \text{... (19)}$$

$$\frac{\kappa_{nf}}{\kappa_f}\theta'' + Pr\left[1-\phi+\phi\frac{(\rho C_p)_s}{(\rho C_p)_f}\right](f\theta'-g\theta)$$
$$+ Br\frac{1}{(1-\phi)^{5/2}}\left[g'^2 + \frac{(\sigma_e)_{nf}}{(\sigma_e)_f}(1-\phi)^{5/2}Mg^2\right] = 0 \qquad \text{... (20)}$$

subjected to the transformed boundary conditions

$$\eta=0: f=f_w, \ g-\lambda g'=1, \ \theta=1$$
$$\eta\to\infty: g\to 0, \ \theta\to 0 \qquad \text{... (21)}$$

The iteration scheme after applying the method strategy is obtained as

$$g''_{r+1} + (1-\phi)^{5/2}\left(1-\phi+\phi\frac{\rho_s}{\rho_f}\right)f_r g'_{r+1} - \frac{(\sigma_e)_{nf}}{(\sigma_e)_f}(1-\phi)^{5/2}Mg_{r+1} \quad \text{... (22)}$$
$$= (1-\phi)^{5/2}\left(1-\phi+\phi\frac{\rho_s}{\rho_f}\right)g_r^2$$

$$f'_{r+1} = g_{r+1} \qquad \text{... (23)}$$

$$\frac{\kappa_{nf}}{\kappa_f}\theta''_{r+1} + Pr\left[1-\phi+\phi\frac{(\rho C_p)_s}{(\rho C_p)_f}\right](f_{r+1}\theta'_{r+1} - g_{r+1}\theta_{r+1})$$
$$+ Br\frac{1}{(1-\phi)^{5/2}}\left[g'^2_{r+1} + \frac{(\sigma_e)_{nf}}{(\sigma_e)_f}(1-\phi)^{5/2}Mg_{r+1}^2\right] = 0$$
$$\text{... (24)}$$

with the initial iteration scheme the boundary conditions

$$\eta=0: f_{r+1}=f_w, \ g_{r+1}-\lambda g'_{r+1}=1, \ \theta_{r+1}=1$$
$$\eta\to\infty: g_{r+1}\to 0, \ \theta_{r+1}\to 0 \qquad \text{... (25)}$$

Following form of the above equations can be obtained by applying Chebyshev pseudo spectral method

$$A_1 g_{r+1} = B_1, g_{r+1}(\tau_N) - \lambda g'_{r+1}(\tau_N)=1, g_{r+1}(\tau_0)=0 \qquad \text{... (26)}$$
$$A_2 f_{r+1} = B_2, f_{r+1}(\tau_N) = f_w \qquad \text{... (27)}$$
$$A_3 \theta_{r+1} = B_3, \theta_{r+1}(\tau_N)=1, \theta_{r+1}(\tau_0)=0 \qquad \text{... (28)}$$
Here,

$$A_1 = D^2 + (1-\varphi)^{5/2}\left(1-\varphi+\varphi\frac{\rho_s}{\rho_f}\right)\text{diag}[f_r]D - \frac{(\sigma_e)_{nf}}{(\sigma_e)_f}(1-\varphi)^{5/2}MI,$$

$$B_1 = (1-\varphi)^{5/2}\left(1-\varphi+\varphi\frac{\rho_s}{\rho_f}\right)g_r^2$$

$$A_2 = D, \ B_2 = g_{r+1},$$

$$A_3 = \frac{\kappa_{nf}}{\kappa_f}D^2 + Pr\left[1-\varphi+\varphi\frac{(\rho C_p)_s}{(\rho C_p)_f}\right]\text{diag}[f_{r+1}]$$

$$D - Pr\left[1-\varphi+\varphi\frac{(\rho C_p)_s}{(\rho C_p)_f}\right]\text{diag}[g_{r+1}]I,$$

$$B_3 = -Br\frac{1}{(1-\varphi)^{5/2}}\left[g_{r+1}'^2 + \frac{(\sigma_e)_{nf}}{(\sigma_e)_f}(1-\varphi)^{5/2}Mg_{r+1}^2\right],$$

subscript r stands for iteration number, diag[ ] is diagonal matrix, I being identity matrix, both of order $(N+1)\times(N+1)$. f, g and θ are the values of function f, g and θ at the mesh points, respectively.

A suitable choice for initial guesses for Eqs (26)–(28)

$$f_0(\eta) = -\frac{\lambda}{2}e^{-\eta/\lambda} + f_w + \frac{\lambda}{2}, \ g_0(\eta) = \frac{1}{2}e^{-\eta/\lambda}, \ \theta_0(\eta) = e^{-\eta} \ ...\ (29)$$

All these initial approximations are chosen at random which satisfies the boundary conditions. Starting from initial guesses, the iterations are solved repeatedly until the desired convergence is achieved, i.e., the following condition is satisfied

$$\max\left\{\|f_{r+1}-f_r\|_\infty, \|g_{r+1}-g_r\|_\infty, \|\theta_{r+1}-\theta_r\|_\infty\right\} < \varepsilon_r \ ...\ (30)$$

here ε_r is the error tolerance which is taken to be at least $\varepsilon_r = 10^{-7}$ in this study.

To accelerate the convergence and to enhance the precision of the spectral relaxation method, a convergence controlling relaxation parameter ω is introduced and employed on Eqs (26)– (28) such that

$$A_1 g_{r+1} = (1-\omega)A_1 g_r + \omega B_1 \qquad\qquad ...\ (31)$$

$$A_2 f_{r+1} = (1-\omega)A_2 f_r + \omega B_2 \qquad\qquad ...\ (32)$$

$$A_3 \theta_{r+1} = (1-\omega)A_3 \theta_r + \omega B_3 \qquad\qquad ...\ (33)$$

with the same boundary conditions Eqs (26)–(28). Here the convergence controlling relaxation parameter ω is taken to be less than unity, i.e., $\omega < 1$.

6 Verification of results

Table 3 demonstrates the validation of computational values of surface heat flux $-\theta'(0)$ for several values of Prandtl number Pr. As a test of precision, the present numerical results are compared with the results by Ishak et al.[47], Mahdy[48] and Rashidi and Abbas[49].

7 Results and discussion

In the present section, the behaviour of dimensionless velocity $f'(\eta)$ and temperature $\theta(\eta)$ are elaborated graphically with various values of physical emerging parameters, suction/injection parameter f_w, velocity slip parameter λ, nanoparticle volume fraction parameter ϕ, magnetic parameter M, Brinkman number Br and empirical shape factor m. Later on, numerical values of the shear stress $f''(0)$ and heat flux $\theta'(0)$ at the surface are also described in tabular form. It is also remarkable that all other parameters are considered to be constant while dealing with anyone of the aforementioned parameter.

Influence of varying values of uniform suction parameter f_w on the fluid flow velocity and temperature are illustrated through Figs 2 and 3, respectively. A growth insuction effect puts a major descend in both the velocity and temperature profiles. Physically, it is clear as due to suction the boundary layer adheres more to the wall and fluid particles are dragged out. This leads to decrease in velocity and momentum boundary layer thickness. This originates a decrement in thickness of boundary layer because fluid gets closer to the wall, which increases the heat transfer rate in consequence.

Figures 4 and 5 displays the influence of velocity slip parameter λ on dimension less velocity and temperature, respectively. A strong deceleration has found in the velocity of the fluid flow with increasing

Table 3 — Comparison of the present numerical values of $-\theta'(0)$ with earlier published data when $f_w = 0 = \lambda = \phi = M = Br$ and $f''(0) = -1.000483$.

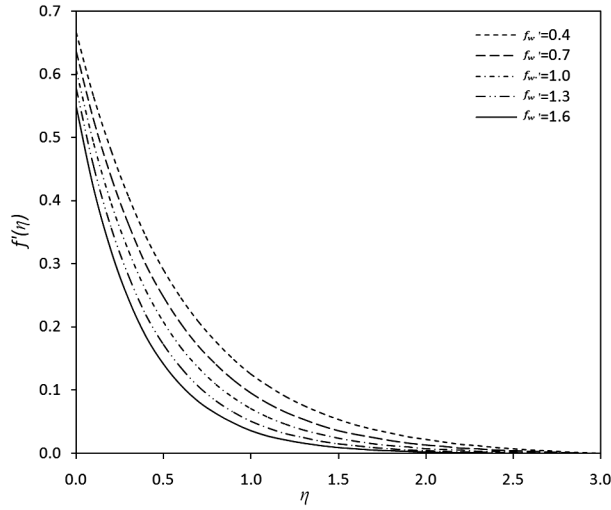| Pr	Ishak et al.[47]	Mahdy[48]	Rashidi and Abbas[49]	Present results
0.72	0.8060	0.80868	0.80883	0.8120664
1.00	1.0000	1.00000	1.00001	1.0004830
3.00	1.9237	1.92368	1.92368	1.9234549
7.00	3.0723	3.07224	3.07225	3.0720790

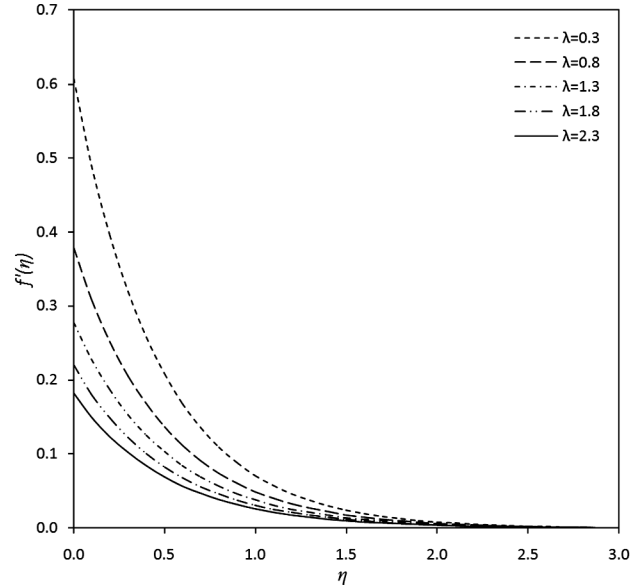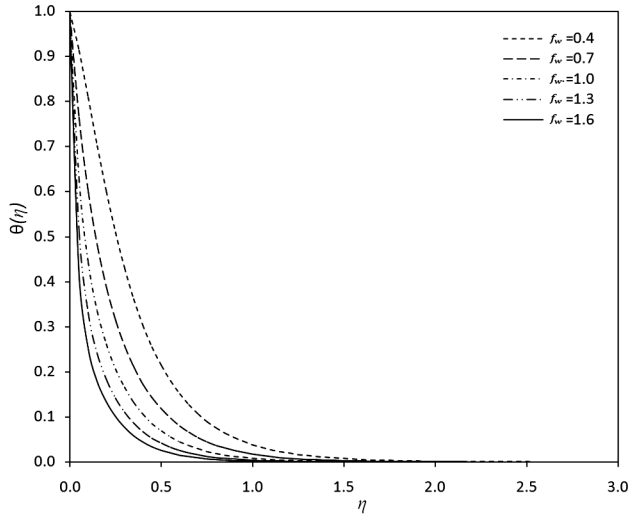Fig. 2 — Effect of f_w on velocity distribution at $\lambda = 0.3$, $\phi = 0.08$ and $M = 1$.

Fig. 3 — Effect of f_w on temperature distribution at $\lambda = 0.3$, $\phi = 0.08$, $M = 1$, $Pr = 25$, $Br = 25$ and sphere-shaped nanoparticle.
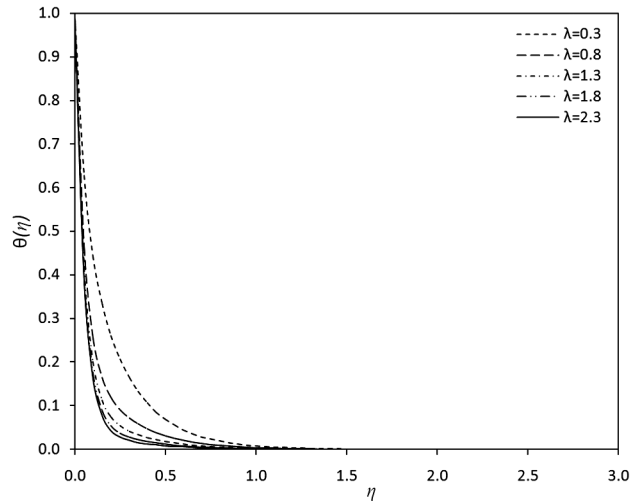

Fig. 4 — Effect of λ on velocity distribution at $f_w = 1.0$, $\phi = 0.08$ and $M = 1$.

Fig. 5 — Effect of λ on temperature distribution at $f_w = 1.0$, $\phi = 0.08$, $M = 1$, $Pr = 25$, $Br = 25$ and sphere-shaped nanoparticle.

values of the slip velocity. It is clear from the Fig. 5 that temperature profile also decreases within the boundary layer region and it confines the thickness of thermal boundary layer. In view of slip condition, the flow velocity adjacent to the surface is no longer identical with the velocity of stretching surface, that results a fall in the fluid flow and temperature.

Impact of nano-particle volume fraction parameter ϕ on the fluid flow $f'(\eta)$ and temperature $\theta(\eta)$ are represented in Figs 6 and 7, respectively. It is observed that the increment in solid volume fraction

parameter leads to reduce the flow velocity, while a slight rise and then a drop for $\eta > 0.5$ in temperature can be seen. From a physical aspect, the fluid becomes more viscous with insertion of more solid particles and hence the nano-fluid velocity decreases while temperature increases due to growth in thermal conductivity. Therefore, enhancement in heat transfer gives rise to temperature.
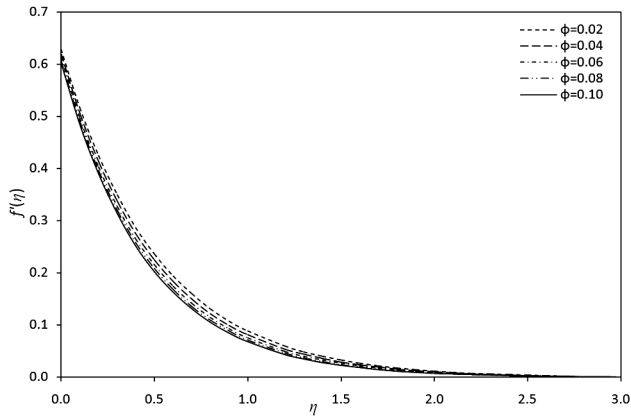
Fig. 6 — Effect of ϕ on velocity distribution at $f_w = 1.0$, $\lambda = 0.3$ and $M = 1$.
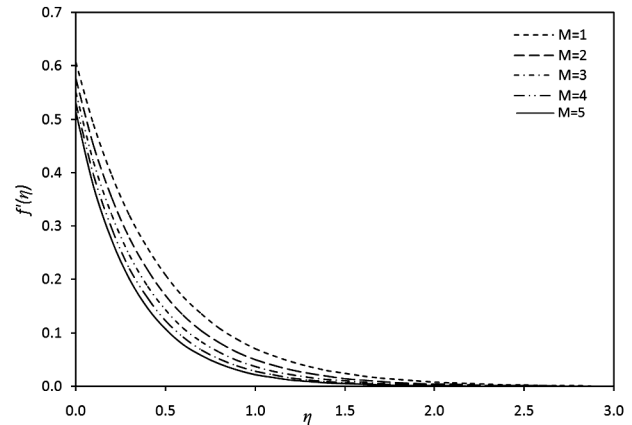

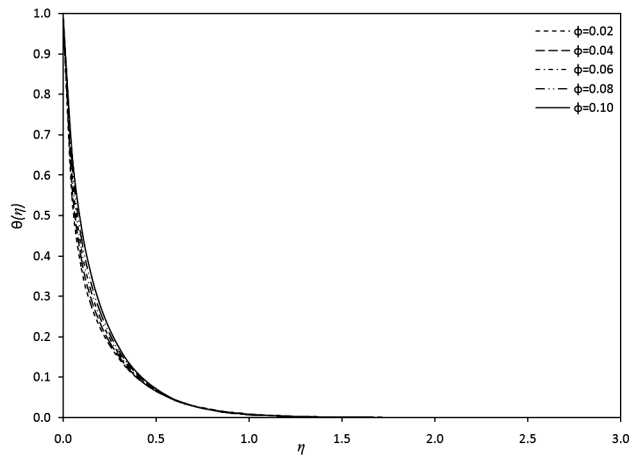Fig. 8 — Effect of M on velocity distribution at $f_w = 1.0$, $\lambda = 0.3$ and $\phi = 0.08$.

Fig. 7 — Effect of ϕ on temperature distribution at $f_w = 1.0$, $\lambda = 0.3$, $M = 1$, $Pr = 25$, $Br = 25$ and sphere-shaped nanoparticle.
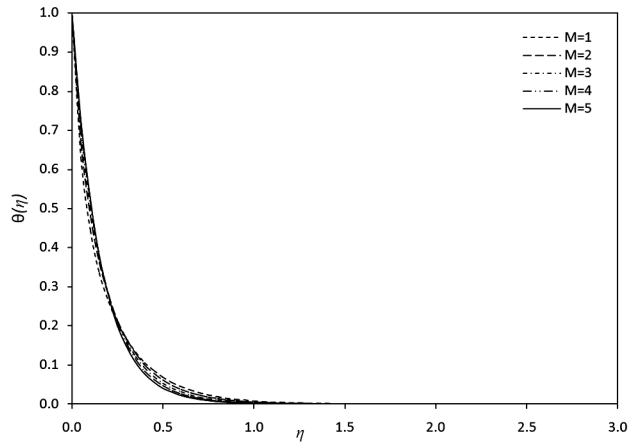

Fig. 9 — Effect of M on temperature distribution at $f_w = 1.0$, $\lambda = 0.3$, $\phi = 0.08$, $Pr = 25$, $Br = 25$ and sphere-shaped nanoparticle.

Figures 8 and 9 demonstrate the variation in dimensionless velocity $f'(\eta)$ and temperature $\theta(\eta)$ with varying magnetic parameter M. It is found that an augmentation in magnetic parameter causes decrease in velocity profile and rise in temperature, while a contrary action is found in the temperature for $\eta > 0.2$. From a physical point of view, it takes place because the implemented magnetic field on electrically conducting nano-fluid creates a resistive force called Lorentz force. This force has a tendency to slow down the motion of the nano-fluid within the boundary layer and consequently velocity reduces due to rise in the magnetic field. Since magnetic parameter is equivalent to the ratio of Lorentz force to viscous force, this leads to rise in resistive force which constitutes more heat.
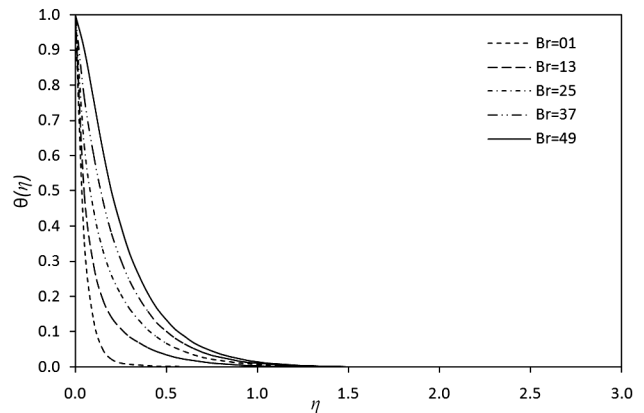

Fig. 10 — Effect of Br on temperature distribution at $f_w = 1.0$, $\lambda = 0.3$, $\phi = 0.08$, $M = 1$, $Pr = 25$ and sphere-shaped nanoparticle.

Figure 10 expresses the behaviour of Brinkman number Br on temperature distribution. The
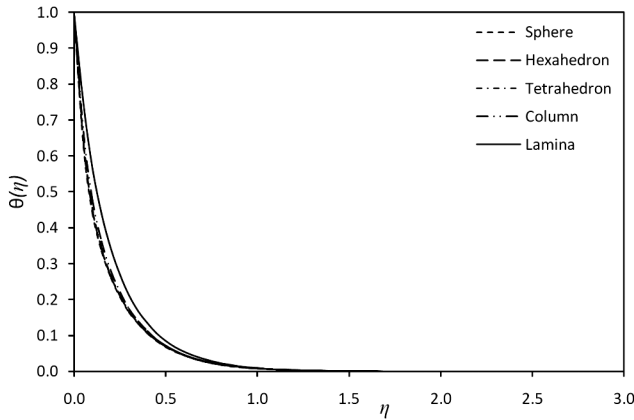
Fig. 11 — Effect of different shaped nanoparticle on temperature distribution at $f_w = 1.0$, $\lambda = 0.3$, $\phi = 0.08$, $M = 1$, $\Pr = 25$ and $Br = 25$.

dimensionless parameter Br is the ratio of heat generated by viscous dissipation to the heat transferred through molecular conduction. Enlargement in Brinkman number gives rise to heat production through viscous dissipation, which raises the fluid temperature and this yields greater buoyancy forces. Hence, enhancement in buoyancy forces along with elevating dissipation parameter causes rise in temperature distribution.

Effects of various nanoparticle shapes, sphere, hexahedron, tetrahedron, cylinder and lamina on the temperature profile $\theta(\eta)$ are depicted in Fig. 11. It is observed that lamina shaped nano particle has a greater influence on enhancement of temperature distribution compared to other shaped nano-particles in sequence of sphere, hexahedron, tetrahedron and cylinder.

Impact of the suction/injection parameter f_w, velocity slip parameter λ, nanoparticle volume fraction parameter ϕ, magnetic parameter M, Brinkman number Br and empirical shape factor m on the surface shear stress and heat transfer rate of the nanofluid are illustrated in Table 4. It is evident from Eq. (16), that the skin friction coefficient C_f and local Nusselt number Nu_x are proportional to the shear stress and heat transfer rate at the surface, respectively. According to the table, skin friction increases with the rising values of velocity slip parameter and decreases with raise in solid volume fraction, magnetic parameter, suction parameter. The table also indicates that local Nusselt number increases with increment in solid volume fraction, magnetic parameter, Brinkman

Table 4 — Numerical values of $-f''(0)$ and $-\theta'(0)$ with impact of different physical parameters at $\Pr = 25$.

f_w	λ	ϕ	M	Br	m	$-f''(0)$	$-\theta'(0)$
0.4	0.3	0.08	1	25	3.000	1.10820020	01.36639
0.7						1.20613380	05.54586
1.0						1.30495660	10.49602
1.3						1.40245830	15.86097
1.6						1.49683860	21.46680
1.0	0.8					0.77534990	16.31123
	1.3					0.55508990	17.99294
	1.8					0.43314220	18.70539
	2.3					0.35541670	19.07005
	0.3	0.02				1.23440570	14.35070
		0.04				1.26275100	12.97880
		0.06				1.28609250	11.69770
		0.10				1.31978130	09.36393
		0.08	2			1.40969750	08.87280
			3			1.49187740	07.76684
			4			1.55952696	06.96685
			5			1.61700048	06.36536
			1	01		1.30495660	20.32123
				13			15.40863
				37			05.58341
				49			00.67080
				25	3.7221		10.03505
					4.0613		09.83337
					6.3698		08.66413
					16.1576		05.86899

number and empirical shape factor, while opposite phenomenon takes place with increasing suction parameter and velocity slip parameter. It is noteworthy that negative values of surface shear stress and heat flux parameter indicate that the fluid makes use of resistive force from the surface and there is a heat effluent from the sheet surface.

8 Conclusions

An overview of MHD boundary layer flow and heat transfer of Cu-blood nanofluid past a stretching sheet has been carried out. Influence of viscous dissipation, Ohmic heating, velocity slip and nanoparticle shape factor has been taken into consideration. The governing boundary system of equations is solved numerically via SRM. The major conclusions from this study can be summarized as follows

(i) Momentum boundary layer thickness diminishes for higher values of suction, velocity slip, solid volume fraction and magnetic parameters.

(ii) Thermal boundary layer thickness and local Nusselt number decrease as suction and velocity slip parameter develop and increase for rising values of solid volume fraction, magnetic parameter and Brinkman number, while opposite phenomenon takes place in the thermal boundary layer for solid volume fraction and magnetic parameter when $\eta > 0.5$ and $\eta > 0.2$, respectively.

(iii) Higher values of velocity slip parameter lead to boost local skin friction coefficient while reverse trend occurs in course of enhancement in suction parameter, volume fraction and magnetic parameter.

(iv) Lamina shaped nanoparticle has a superior effect on rising fluid temperature and local Nusselt number compared to remaining particle shapes.

References

1 Abo-Eldahab EM & El Aziz MA, *Appl Math Model*, 29 (2005) 579.
2 Palani G & Kim K Y, *J Eng Thermophys*, 20 (2011) 501.
3 Hayat T, Imtiaz M & Alsaedi A, *Adv Powder Technol*, 27 (2016) 1301.
4 Chaudhary S & Choudhary M K, *Eng Comput*, 35 (2018) 1675.
5 Aly EH & Pop I, *Powder Technol*, 367 (2020) 192.
6 Zhang X H, Abidi A, Ahmed A E, Khan M R, El-Shorbagy M A, Shutaywi M, Issakhov A & Galal AM, *Case Stud Therm Eng*, 26 (2021) 101184.
7 Alfvén H, *Nature*, 150 (1942) 405.
8 Abo-Eldahab E M & Salem AM, *Appl Math Comput*, 169 (2005) 806.
9 Rashidi M M, *Comput Phys Commun*, 180 (2009) 2210.
10 Kechil SA & Hashim I, *Commun Nonlinear Sci Numer Simul*, 14 (2009) 1346.
11 Jat RN & Chaudhary S, *Z Angew Math Phys*, 61 (2010) 1151.
12 Misra JC & Sinha A, *Heat Mass Transf*, 49 (2013) 617.
13 Chaudhary S & Kumar P, *Meccanica*, 49 (2014) 69.
14 Mabood F, Khan WA & Ismail AM, *J Magn Magn Mater*, 374 (2015) 569.
15 Khan U, Ahmed N, Mohyud-Din ST & Bin-Mohsin B, *Neural Comput Appl*, 28 (2017) 2041.
16 Abdel-Wahed M S & Emam T G, *Therm Sci*, 22 (2018) 857.
17 Waini I, Ishak A & Pop I, *Appl Math Mech*, 41 (2020) 507.
18 Martin MJ & Boyd I D, *Chem Eng Commun*, 20 (2006) 710.
19 Zhu J, Zheng L C & Zhang Z G, *Appl Math Mech*, 31 (2010) 439.
20 Seth G S & Mishra M K, *Adv Powder Technol*, 28 (2017) 375.
21 Chaudhary S & Choudhary M K, *Therm Sci*, 22 (2018) 797.
22 Tabassum M & Mustafa M, *Int J Heat Mass Transf*, 123 (2018) 979.
23 Murthy M K, *Indian J Phys*, 94 (2020) 2023.
24 Choi S U & Eastman J A, *Mater Sci*, 231 (1995) 99.
25 Xuan Y & Li Q, *J Heat Transf*, 125 (2003) 151.
26 Khanafer K, Vafai K & Lightstone M, *Int J Heat Mass Transf*, 46 (2003) 3639.
27 Gümgüm S & Tezer-Sezgin M Ü, *Eng Anal Bound Elem*, 34 (2010) 727.
28 Khan WA & Pop I, *Int J Heat Mass Transf*, 53 (2010) 2477.
29 Mahmoodi M & Hashemi S M, *Int J Therm Sci*, 55 (2012) 76.
30 Sheikholeslami M, Hatami M & Ganji D D, *Powder Technol*, 246 (2013) 327.
31 Turkyilmazoglu M, *J Heat Transf*, 137 (2015) 024501.
32 Su X, *Indian J Pure Appl Phys*, 55 (2017) 564.
33 Daniel Y S, Aziz Z A, Ismail Z & Salah F, *Alex Eng J*, 57 (2018) 2187.
34 Chaudhary S & Kanika K M, *Phys Scr*, 95 (2019) 025202.
35 Cortell R, *Appl Math Comput*, 168 (2005) 557.
36 Ibrahim W & Shankar B, *Comput Fluids*, 75 (2013) 1.
37 Khader M M & Megahed A M, *J Appl Mech Tech Phys*, 56 (2015) 241.
38 Khan M, Shahid A, Malik M Y & Salahuddin T, *J Mol Liq*, 251 (2018) 7.
39 Nadeem S & Khan A U, *Phys Scr*, 94 (2019) 075204.
40 Chaudhary S & Kanika K M, *J Porous Media*, 23 (2020) 27.
41 Jabeen K, Mushtaq M & Akram R M, *Math Probl Eng*, 2020 (2020) 1.
42 Jafari S S & Freidoonimehr N, *J Braz Soc Mech Sci Eng*, 37 (2015) 1245.
43 Dinarvand S, Rostami M N, Dinarvand R & Pop I, *Int J Numer Methods Heat Fluid Flow*, 29 (2019) 4408.
44 Tripathi D, Prakash J, Tiwari A K & Ellahi R, *Microvasc Res*, 132 (2020) 104065.
45 Mohammad R & Kandasamy R, *J Mol Liq*, 237 (2017) 54.
46 Motsa S S, *Chem Eng Sci*, 201 (2014) 241.
47 Ishak A, Nazar R & Pop I, *Meccanica*, 44 (2009) 369.
48 Mahdy A, *Nucl Eng Des*, 249 (2012) 248.
49 Rashidi M M & Abbas M A, *Entropy*, 19 (2017) 414.